Journal of ELECTRONIC MATERIALS, Vol. 49, No. 1, 2020
https://doi.org/10.1007/s11664-019-07669-7

The Growth of Interfacial IMC Layer in SAC0307 Solder Joints with Specific Grain Orientation Under Electrical and Thermal Coupling Fields

YU TIAN,[1] LIMIN MA,[1,2,3] YISHU WANG,[1,2] FU GUO,[1,2,4] and ZHIJIE SUN[1]

1.—College of Material Science and Engineering, Beijing University of Technology, Beijing 100124, People's Republic of China. 2.—Key Laboratory of Advanced Functional Materials, Education Ministry of China, Beijing University of Technology, Beijing 100124, People's Republic of China. 3.—e-mail: malimin@bjut.edu.cn. 4.—e-mail: guofu@bjut.edu.cn

We reported the reliability of Sn0.3Ag0.7Cu (SAC0307) solder joints under electrical and thermal coupling fields, where the *c*-axes of Sn grains were all nearly parallel to the direction of current and thermal flows. In these studies, individual electromigration (EM), individual thermomigration (TM), and thermoelectric coupling migration behaviors were investigated by applying a current density of 10^4 A/cm^2, and a temperature gradient of 10^3°C/cm at Cu/SAC0307/Cu solder joints, respectively. The SEM and EBSD were utilized to characterize the morphologies and crystal orientations of each solder joint. The results indicated that the Cu atoms tended to migrate to the anode side under EM. The thickness of an interfacial intermetallic (IMC) layer at the anode increased 3.93 μm. In addition, the Cu atoms diffused toward the lower temperature side under TM, and the thickness of the IMC layer at cold side increased 1.72 μm. When the solder joints were experiencing the coupling fields with the same directions of current and thermal flows, the thickness of IMC layer at anode side (cold side) could increase up to 7.67 μm. The results showed that the effect of thermal flow could assist to accumulate the IMC at the anode side, and accelerate the migration of Cu atoms. This research could help to further understand the reliability behaviors of SAC0307 solders under the service environment.

Key words: SAC0307 solder joint, thermoelectric coupling, grain orientation, IMC growth behavior

INTRODUCTION

The arrival of the information age leads to the rapid development of electronic packaging technology.[1] The development of integrated circuit technology makes the function in the package slowly change. The attention of users is often not the quality of the chip, but the reliability of the whole package which is connected by chips and package material.[2] The electronic connection technology may be directly related to the performance of the chip, which is essential to the reliability of electronic components. So the reliability of solder joints has been the most concerned issue for the whole electronic packaging industry.[3,4] The EM of solder joints under high current stressing has been regarded as the main reliability concern in microelectronic devices due to the miniaturization and the requirements for enhanced performance of devices.[5–7] The size of solder joints continuously decreases, resulting in the extremely increased current density.[4,8] Under EM, voids, phase separation, crystal whisker growth, and cracks propagation would emerge and thereby accelerate the

(Received April 24, 2019; accepted September 21, 2019; published online October 16, 2019)

failure of solder joints.[6,9] In addition, heat generated due to joule heating during EM, might cause a temperature gradient in solder joints. Previous studies theoretically deduced that when the thermal gradient is large enough, it can be the dominant driving force.[10–12] TM is a mass migration of compound material caused by a temperature gradient.[13] Rimbey et al. indicated that the electronic contribution to the driving force for TM in metals is considered within the linear- response formalism.[14–16] In addition, there are two additional contributions to TM. One of these is the phonon contribution, which arises from the stream of phonons that is generated by the temperature gradient and is subsequently scattered by the impurity. There is also the so-called intrinsic contribution, which arises from the effects of a temperature gradient on the diffusion dynamics rather than on the electronic carriers.[4,17,18] And Jones et al. has used general linear response theory to provide a set of correlation functions for determining the electronic contribution to the driving force on an ion in a thermal gradient.[19] Gillian et al. has used a molecular dynamics simulation to evaluate Green–Kubo relations for the TM of hydrogen in palladium, obtaining qualitative agreement with experiment.[20]

Recently, the TM of solder joints has been reported to accompany EM in flip chip solder joints. What is more, an FE simulation result supports the existence of the temperature gradient.[4,18] TM might assist or counter EM depending on the direction of the temperature gradient and electric field.[21] Ye et al. was the first to show that TM forces under high current density can be larger than EM in flip chip solder joints.[4] A temperature difference of 15°C across a 100 μm diameter solder joint would produce a temperature gradient of 1500°C/cm, which would cause TM in solder joints.[22–24] Huang et al. observed a migration of the Sn-rich phase owing to EM and TM in tin–lead composite solder joints.[25] However, the increasingly severe environment problems lead to the widely used Sn-based lead-free solder. Therefore, the reliability issues related to lead-free solder have attracted significant attention in the microelectronics industry.[26,27] Guo et al. studied that elevated temperature and sufficient temperature gradient were the two major factors that caused TM.[28] Previous studies found that the Bi atoms migrated to the lower temperature side driven by the temperature gradient.[5,29] However, the phase separation in Sn58Bi solder joint is the important problem to solve in EM and TM.[30,31] SAC0307 has become one of the most highly potential solders due to the better properties and lower price than other solder.[32] Both of EM And TM are the main factors leading to the failure of solder joints. In this paper, the individual EM and TM behaviors in SAC0307 solder joints are investigated systematically. In addition, the thermoelectric coupling behavior is also discussed with different relations between EM and TM.

EXPERIMENTS

SAC0307 lead-free solder paste was used in this study. The copper strips with the dimension of 0.5 mm × 0.3 mm × 5 mm were used to fabricate the linear butt weld solder joints. Figure 1 showed the schematic diagram of the specimen. After grounding the cross section of the copper strips, acetone and 30% nitric acid solution were used to clean the copper strips for 10 min. The SAC0307 solder was filled in the predesigned soldering seam between two copper strips, and the soldering seam was about 100-120 μm. The specimens were placed in a reflow furnace for 4 min and the peak temperature was 245°C. And then the solder joints were cooled in the air. After removing the excessive solder, the solder joints were mounted on the 10 mm × 10 mm × 1.5 mm printed circuit boards (PCB) by epoxy resin. The observed surfaces of the solder joints were with the dimension of 500 μm × 100 μm. All of the joints were subjected to a metallographic grinding and polishing process with 0.05 μm Al_2O_3 supensions for characterization before EM and TM experiments. A constant current density of 10^4 A/cm^2 was continously applied to the solder joints at room temperature. At the same time, heat was applied at one of the end of the solder joint, and a heat sink was applied at another end. Thus, the solder joints were subjected to a temperature gradient of 10^3°C/cm for TM. The schematic drawing of EM and TM test is shown in Fig. 2. The microstructure evolution of the solder joints was characterized by scanning electron microscopy (SEM) equipped with an electron back-scattered diffraction (EBSD) by the *in situ* observation. The composition of the solder joints were studied by an Energy Dispersive Spectrometer (EDS). The thickness of IMC layer at the interface was measured by Photoshop® software.

RESULTS AND DISCUSSION

Eletromigration Behavior

Figure 3a and b show the initial EBSD orientation map and pole figures of Sn grains in SAC0307 solder joint, S1. The tetragonal frame represented the unit cell of Sn grain. For the EBSD maps, red

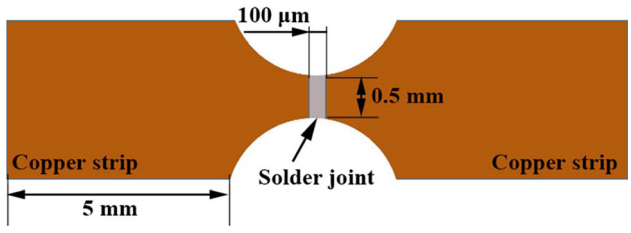

Fig. 1. A schematic drawing of line-type solder joints.

lines represent high-angle grain boundaries (larger than 15°) and blue and green lines represent the low-angle subgrain boundaries (larger than 2° but < 15°). The electron flow direction is from left side to right side, as shown by the white arrow. The angle between *c*-axis direction and the electron flow direction is nearly 7.8°. Moreover, the pole figures also are consistent with EBSD results. Thus, the *c*-axis direction of Sn grain could be considered nearly parallel to the direction of electron flow.

Figure 4 shows the interfacial microstructures of S1 at the anode and the cathode after high current stressing for 0 day, 3 days, and 6 days. After reflow, a little primary phase of Cu_6Sn_5 particles generated at the solder matrix, and dispersed randomly. In addition, the discontinuous scallop-shaped Cu-Sn IMC layers were formed between the Cu strips and the SAC0307 solder matrix. Figure 5 indicates the evolution columnar of the average thickness of IMC layers with different EM times. The average thickness of IMC layers at anode and cathode were measured as 3.96 μm and 3.93 μm, respectively. After current stressing for 3 days, the average thickness of an anode IMC layer was 5.73 μm, and the average thickness of a cathode IMC layer increased slightly. With the increasing of EM time, the average thicknesses of anode and cathoder IMC layers were 7.89 μm and 3.88 μm, respectively. The thickness of anode IMC layer continuously increased. The morphology of IMC layers transformed from discontinous to continuous irregular-shaped. During EM, the concentration gradient between Cu strip and solder matrix provide the Cu atoms flux form Cu strip to the solder matrix, which lead to the slight increase of the thickness of the cathode IMC layer. Moreover, due to the Cu atoms preferred migration along the *c*-axis, the Cu atoms moved from cathode to anode easily and quickly. Under the effect of high current stressing, the driving force by the electron is stronger than the driving force induced by concentration gradient. And the J_{EM} is larger than J_C.

$$J_{EM} = C\frac{D}{KT}Z^*e\rho j, \quad (1)$$

where D is the diffusion coefficient, K is the Boltzmanns constant, T is the absolute temperature, Z^* is the effective charges, e is the electron charge, ρ is the resistivity, and j is the current density.[33]

In addition, during the process of migration of Cu atoms, the Cu atoms reacted with Sn atoms to form

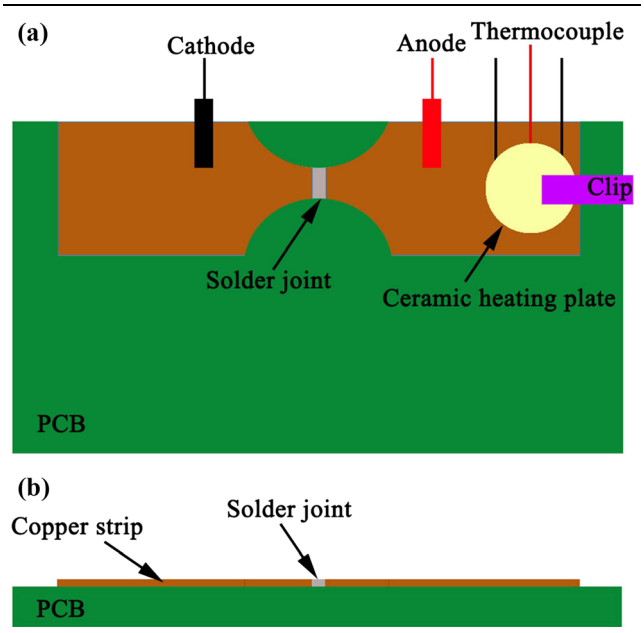

Fig. 2. The schematic drawing of thermoelectric coupling experimental platform (a) top view, (b) side view.

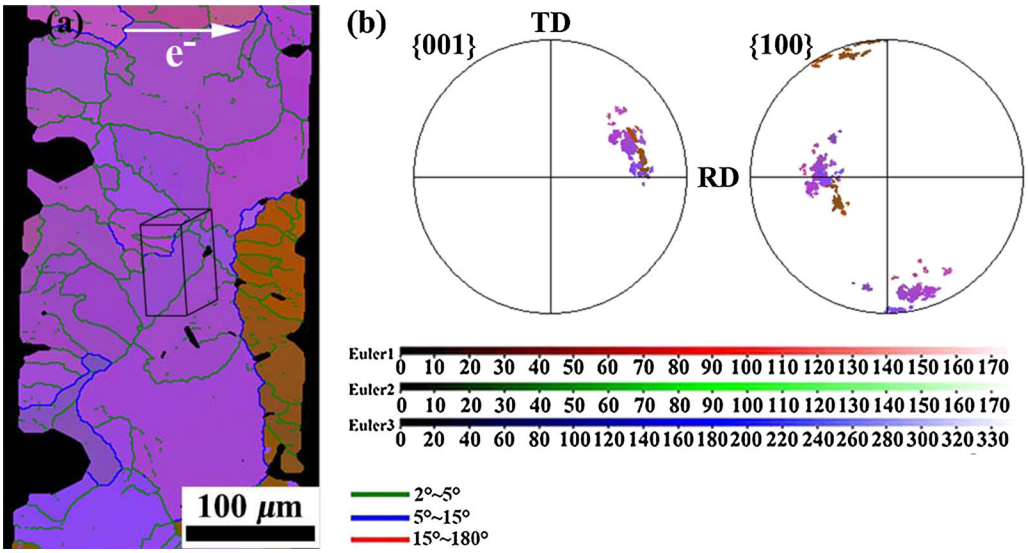

Fig. 3. The crystal orientation of reflowed S1 (a) EBSD orientation map; (b) (001) and (100) plane figures.

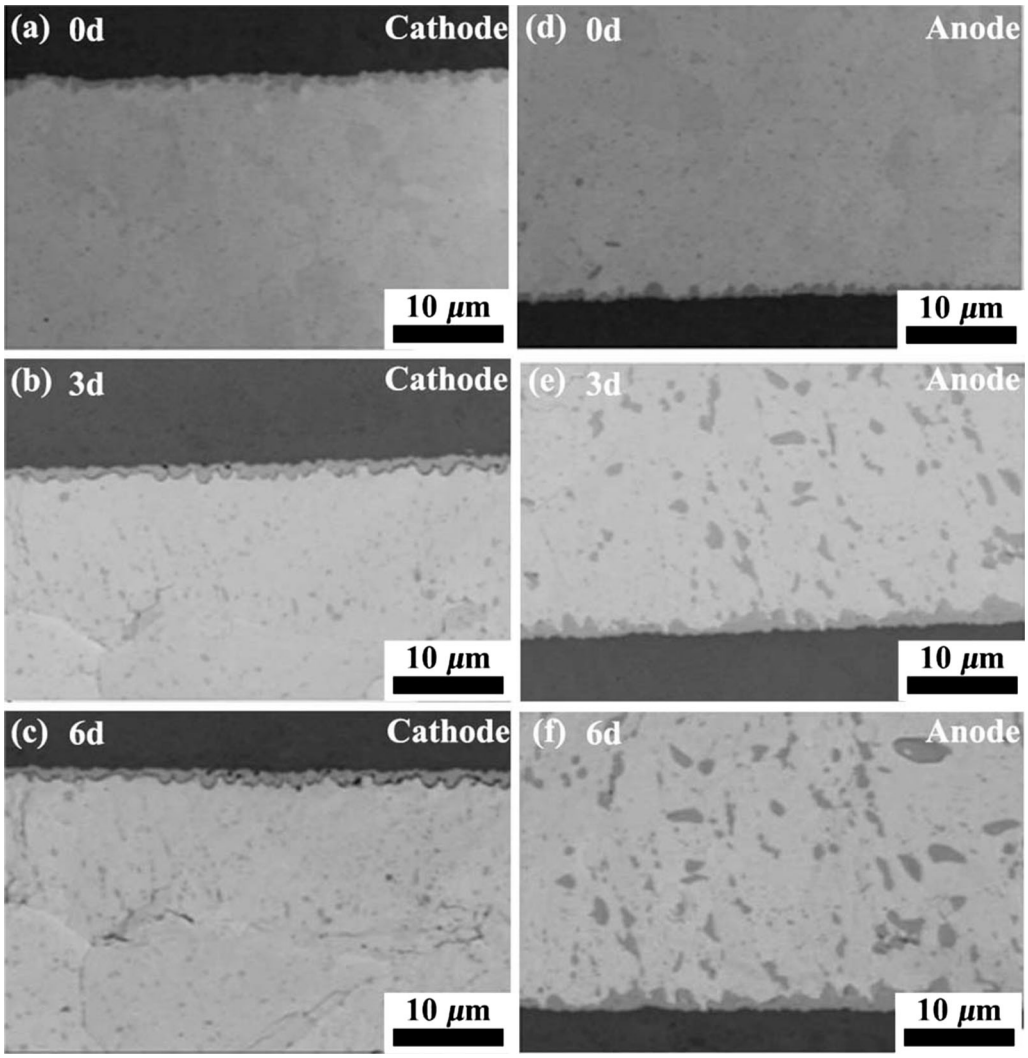

Fig. 4. EM images of microstructure evolution of interfacial IMC layers after different EM time of S1 (a, d) 0 d; (b, e) 3 d; (c, f) 6 d.

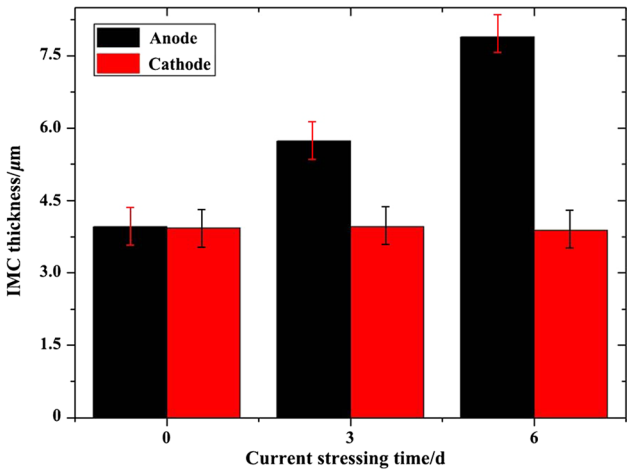

Fig. 5. The average thickness of interfacial IMC layers after different EM times of S1.

IMCs in the solder matrix. So the IMCs in solder matrix grew up, and the size of IMCs were lager than the reflowed state in S1.

Thermomigration Behavior

Figure 6a shows the EBSD orientation map of Sn grains in S2. The tetragonal frame represented the unit cell of Sn grain in S2. Figure 6b shows the different directions of pole figures in S2. The left side is the hot side, and the right side is the cold side, which indicates that the temperature gradient is from left side to right side, as shown in Fig. 7. The angle between *c*-axis direction and the temperature gradient direction is calculated as 3.65°. Thus, the relationship between the *c*-axis and the temperature gradient is nearly parallel to each other.

The interfacial microstructures of S2 at hot side and cold side after suffering TM for 0 days, 3 days,

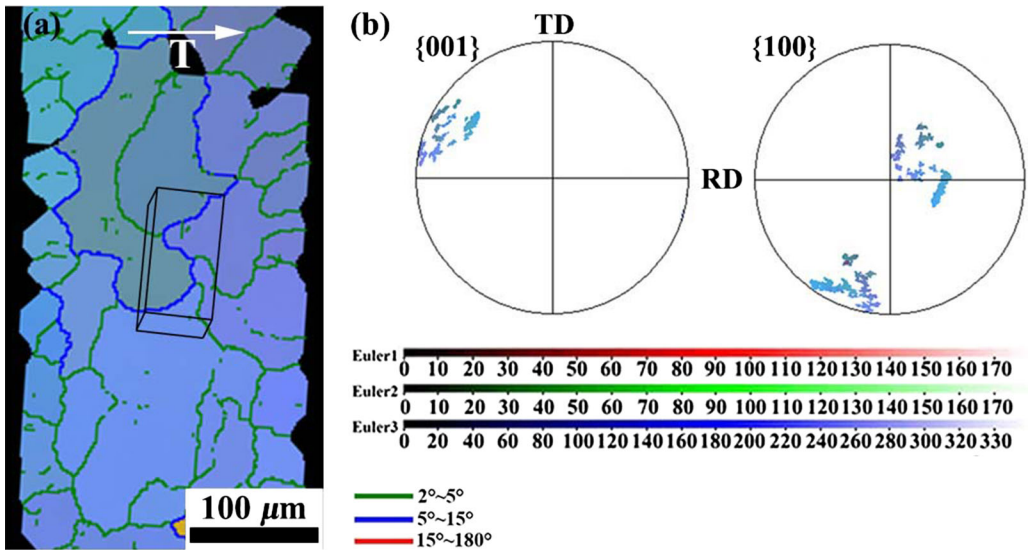

Fig. 6. The crystal orientation of reflowed S2 (a) EBSD orientation map; (b) (001) and (100) plane figures.

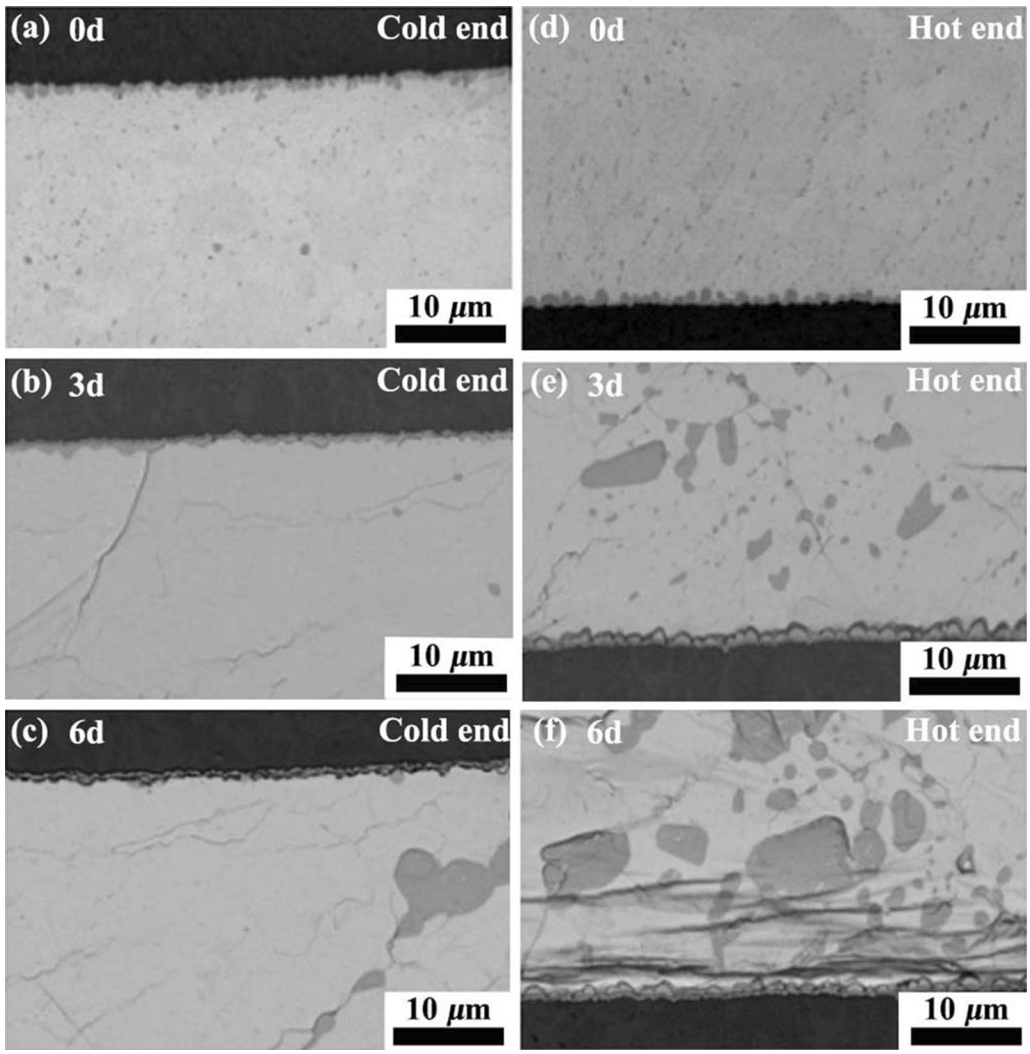

Fig. 7. EM images of microstructure evolution of interfacial IMC layers after different TM time of S2 (a, d) 0 d; (b, e) 3 d; (c, f) 6 d.

and 6 days are shown in Fig. 7a, b, c, d, e, and f. After reflow, the IMC layers formed at the interfaces between the solder matrix and copper stripes. The average thicknesses of hot side and cold side were 3.95 μm and 3.96 μm, respectively. What is more, the IMCs dispersed randomly at the solder matrix. With the increasing of TM time, the IMCs near to the cold side grew up and gathered at the cold side. In addition, the average thickness of the hot side is 3.98 μm, and the morphology of the IMC layer becomes flattened. However, the IMC layer at the cold side becomes more irregular, and the average thickness increases sharply, as shown in the evolution columnar of IMC layer thickness of Fig. 8. The temperature gradient is from hot side to cold side, the Cu atoms diffuse by the driving force of TM from hot side to cold side. After TM for 6 days, the average thickness of cold side IMC layer continuously increased to 5.68 μm, and thickness of the IMC layer at hot side decreased to 3.93 μm. In addition, the size of IMCs near to the cold side is larger than that of before TM.

Hsiao reported that the homogeneous solid phase could be changed into non-homogeneous phase under TM.[34] And this process requires that the direction of uphill diffusion is opposite to the component concentration gradient. Thus, the direction of TM is opposite to the concentration gradient, and the net atomic flux, J_{net} can be expressed as:

$$J_{\text{net}} = J_{\text{C}} + J_{\text{TM}}, \tag{2}$$

$$J_{\text{TM}} = D\frac{\mathrm{d}T}{\mathrm{d}x}, \tag{3}$$

where the $\mathrm{d}T/\mathrm{d}x$ is the temperature gradient. And $J_{\text{C}} > 0$ due to the diffusion of Cu atoms is the uphill diffusion. At the hot side, the Cu atoms migrated from the Cu strip to the solder matrix, which leads to the slight increase of the thickness of IMC layer at the hot side. In addition, the initial IMC layer formed during reflow was decomposed by the concentration gradient, so the Cu atoms migrated from the hot side to the cold side. And the thickness of the IMC layer at hot side would decrease with the increasing of TM time. The results indicate that the effect of the decomposition is stronger than the effect of concentration gradient.

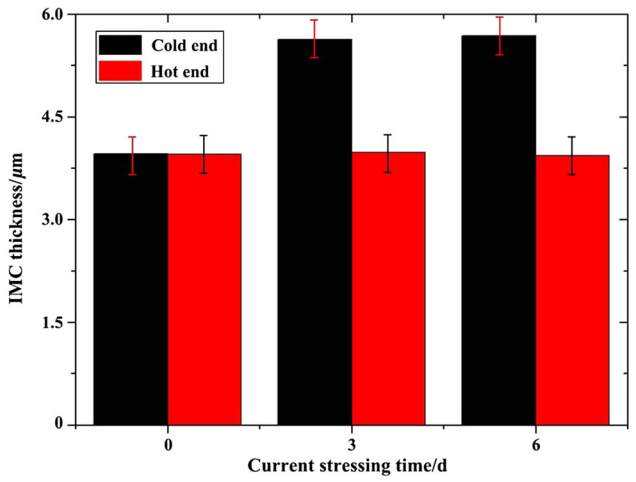

Fig. 8. The average thickness of interfacial IMC layers after different TM times of S2.

Thermoelectric Coupling Behavior

The direction of electron flow was from left side to right side, named + E_{D}. Moreover, the hot side is the left side, and the cold side is the right side. So, the temperature gradient was from the hot side to cold side, named + T_{D}.

+ E_D *and* + T_D

Figure 9 shows the EBSD orientation of S3 that was subjected to the thermoelectric coupling conditions. The tetragonal frame represented the orientation of different Sn grains. The angle between *c*-axis and electron flow was 4.05°. Therefore, the *c*-axis of Sn was nearly parallel to the electron flow.

Figure 10 shows the anode and the cathode interfacial microstructure evolution of S3 for different thermoelectric coupling times. And the initial thickness of IMC layers at the anode and the cathode side were measured to have an average thickness of 3.89 μm and 3.88 μm, respectively. After thermoelectric coupling for 3 days, the thickness of the IMC layer at anode and cold side was 7.86 μm. With the increasing of thermoelectric coupling time until 6 days, the thickness of IMC layer at anode and cold side increased up to 11.56 μm. Moreover, the morphology of the IMC layer at anode and cold side transformed to a planar layered structure. However, the copper strip at cathode and hot side had been consumed under the effect of EM and TM, and the interface between the copper strip and solder matrix migrated to the copper strip at the cathode and hot side from the original position after reflow. So the thickness of the IMC layer could not be measured. The IMC layer morphology also became more uneven. Figure 11 indicates that the evolution columnar of IMC layer thickness with various periods of thermoelectric coupling times. What is more, the surface morphology of the solder joint became more irregular. There were some Cu_6Sn_5 protruding form the solder matrix closed to the anode and cold side. And there were the same cracks formed near the cathode and hot side.

The electron wind force and temperature gradient were the main driving forces which lead to the polarization effect under thermoelectric coupling conditions. On the one hand, when the *c*-axis is parallel to the electron flow, the metal atoms have the largest diffusion. The IMC layer at the cathode was consumed and Cu atoms migrated to the anode under the effect of electron wind force. As a result, the IMC layer thickness increased fast at the anode.

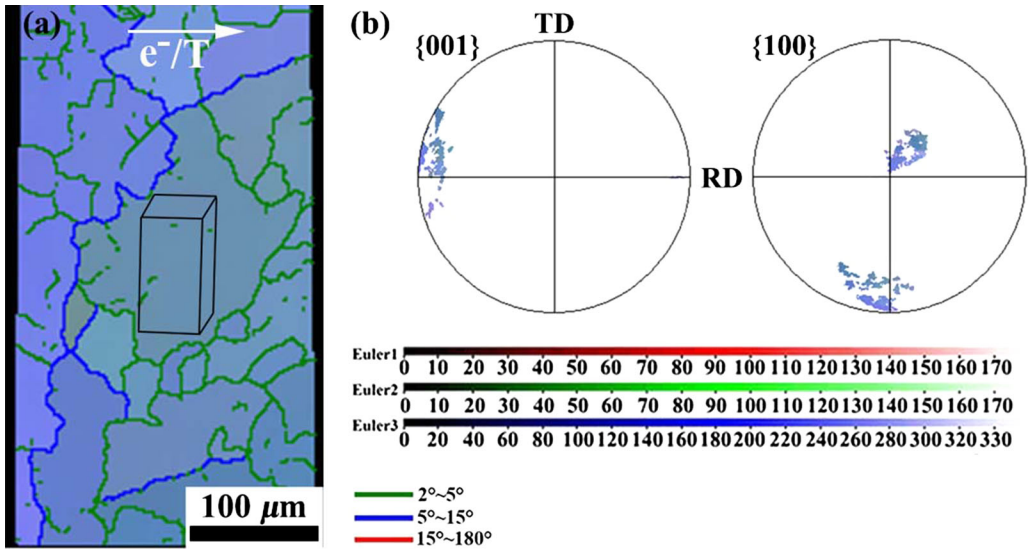

Fig. 9. The crystal orientation of reflowed S3 (a) EBSD orientation map; (b) (001) and (100) plane figures.

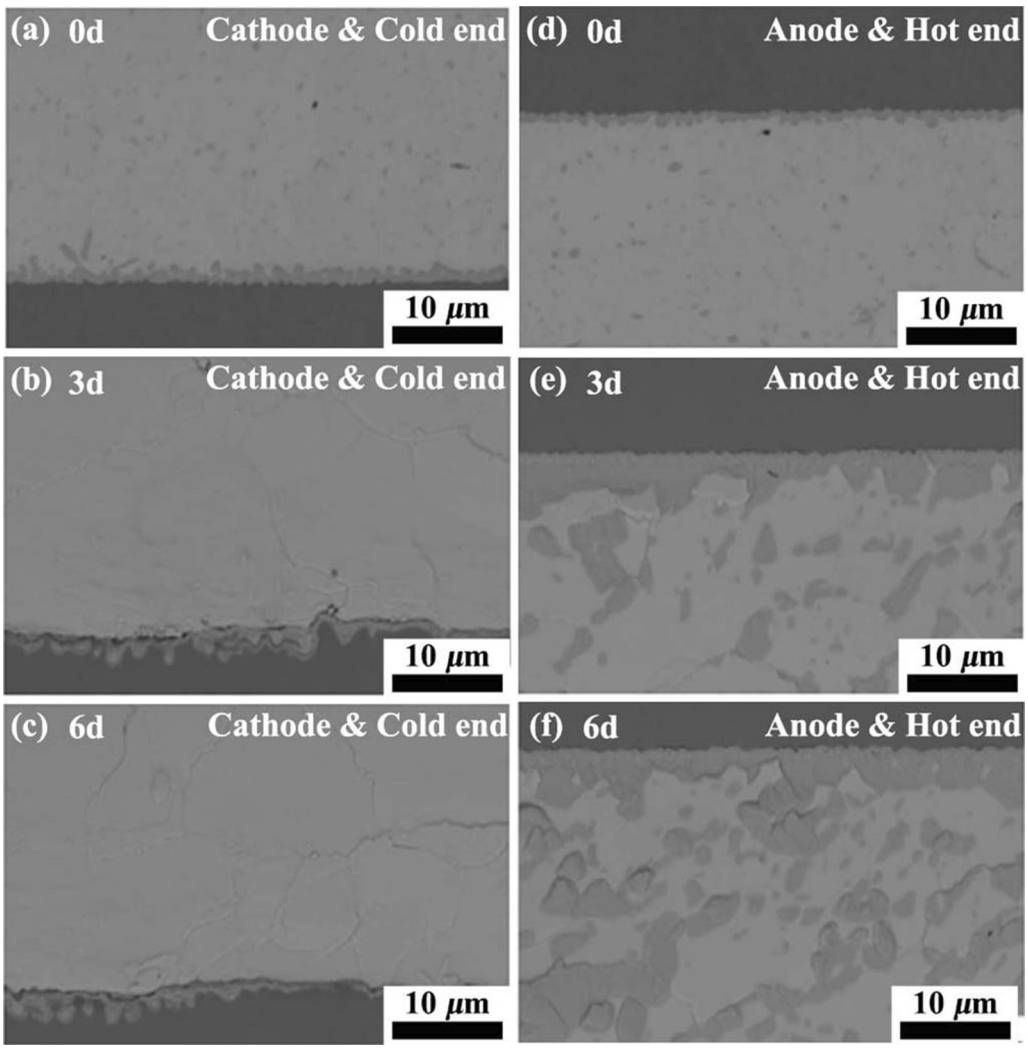

Fig. 10. EM images of microstructure evolution of interfacial IMC layers after different EM coupling TM time of S3 (a, d) 0 d; (b, e) 3 d; (c, f) 6 d.

During the process of migration, Cu and Sn atoms reacted and formed Cu_6Sn_5 in a solder matrix. In addition, the protrusion of Cu_6Sn_5 at the solder matrix could release the stress of the solder matrix, and decreased the surface energy. On the other hand, the temperature gradient accelerated the diffusion of Cu atoms from hot side to cold side, which promoted the formation of IMC at the interface between the cold side and solder matrix. Due to the direction of electron flow and the direction of temperature gradient having the same directions, the atomic migration flux caused by electron wind force (J_{EM}) and temperature gradient (J_{TM}) could promote each other, which could be expressed as the following formulas:

$$J^{Cu}_{\text{anode and cold end}} = J^{Cu}_{EM} + J^{Cu,}_{TM} \quad (4)$$

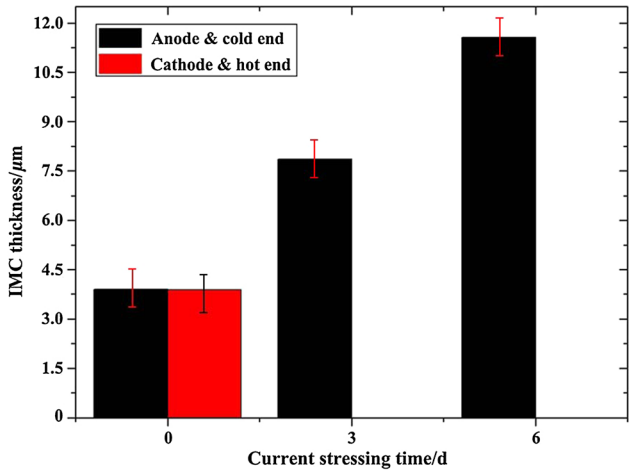

Fig. 11. The average thickness of interfacial IMC layers after different EM coupling TM time of S3.

$$J^{Cu}_{\text{cathode and hot end}} = -J^{Cu}_{EM} - J^{Cu}_{TM}. \quad (5)$$

Combined with the formulas, it indicated that the thickness of the IMC layer at anode and cold side became more and more thicker. Because the diffusive fluxes of Cu atoms from cathode and hot side to the anode and cold side were J_{EM} and J_{TM}. As a result, the Cu atoms accumulated at the anode and cold side, leading to formation of planar layered structure of the IMC layer at the interface. However, the IMC layer at the cathode and hot side was consumed with the increase of thermoelectric coupling times. At the cathode and hot side, the Cu atoms migrated to anode and cold side, leading to the lack of Cu atoms. The copper strip provided the limitless supplement of Cu atoms for the EM and TM, so the position of the IMC layer at the cathode and hot side had changed. Hence, under the double effects of electron wind force and temperature gradient, the polarization effect becomes more serious than the single effect of EM or TM when the direction of electron flow is parallel to c-axis direction.

$+E_D$ and $-T_D$

Figure 12 shows the EBSD orientation of S4 that the c-axis of Sn was nearly parallel to the electron flow direction. And the angle between c-axis and electron flow was calculated as 4.24°. Figure 13 shows the anode and cathode interfacial microstructure evolution of sample 3 for different thermoelectric coupling times. The interfacial IMC layers formed at the anode (hot side) and the cathode (cold side) after reflow, and the original average thickness of the IMC layer were 3.90 μm and 3.89 μm, respectively. Moreover, the eutectic primary phase also formed and randomly distributed at the solder matrix. The evolution columnar of IMC layer

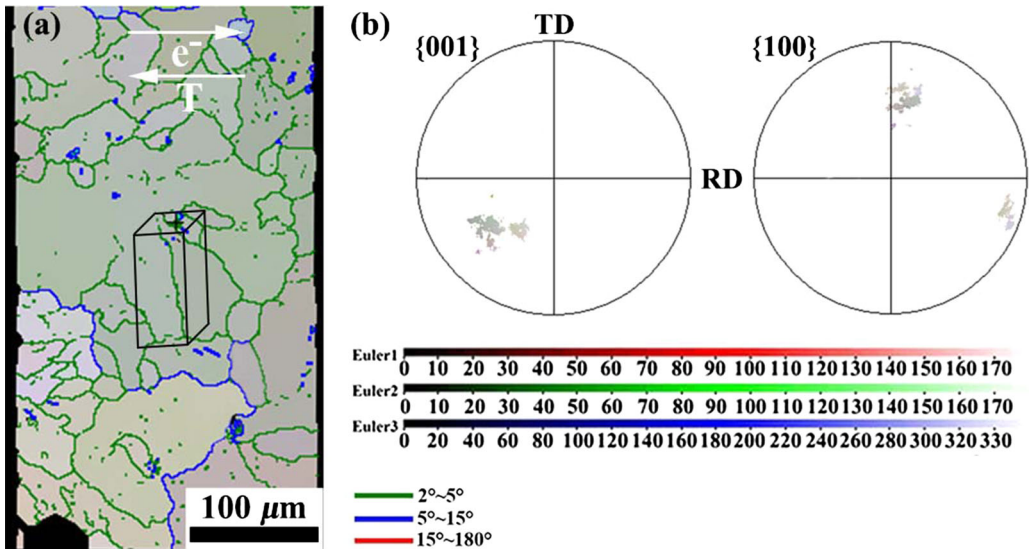

Fig. 12. The crystal orientation of reflowed S4 (a) EBSD orientation map; (b) (001) and (100) plane figures.

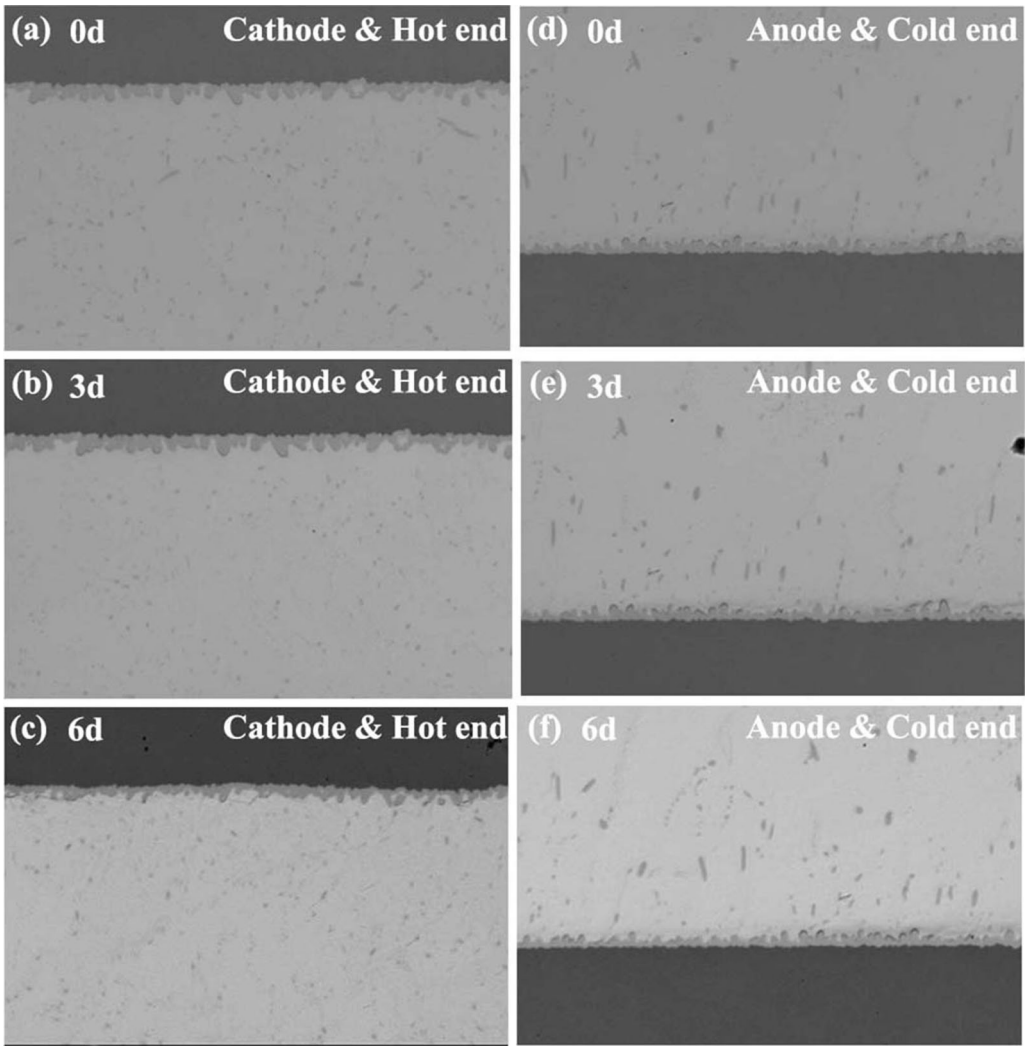

Fig. 13. EM images of microstructure evolution of interfacial IMC layers after different EM coupling TM time of S4 (a, d) 0 d; (b, e) 3 d; (c, f) 6 d.

thickness is shown in Fig. 14. Under the effect of electron wind force, the metal atoms migrated from the cathode to the anode, which caused the increase of IMC layer thickness at the anode, and the decrease of the cathode IMC layer thickness. In addition, the atoms migrated from the hot side to the cold side by the driving force of TM under the temperature gradient condition. As a result, the IMC layer thickness at the cold side and at the hot side slightly changed. Moreover, under the thermo-electric coupling conditions, the atomic migration flux could be expressed as:

$$J^{\mathrm{Cu}}_{\text{anode and hot end}} = J^{\mathrm{Cu}}_{\mathrm{EM}} - J^{\mathrm{Cu}}_{\mathrm{TM}}, \tag{6}$$

$$J^{\mathrm{Cu}}_{\text{cathode and cold end}} = -J^{\mathrm{Cu}}_{\mathrm{EM}} + J^{\mathrm{Cu}}_{\mathrm{TM}}, \tag{7}$$

thus, at the anode and hot side, the final atomic migration flux was offset from each other by J_{EM}

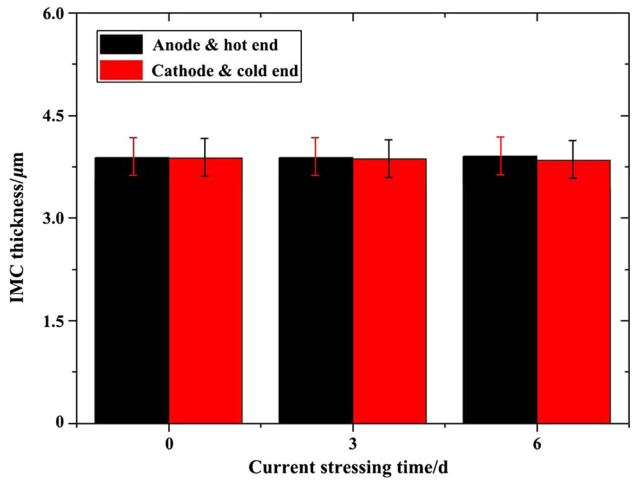

Fig. 14. The average thickness of interfacial IMC layers after different EM coupling TM times of S4.

and J_{TM}. As a result, the thickness of IMC layer at anode and hot side increased for 0.2 μm. However, at the cathode and cold side, the IMC layer thickness decreased for 0.3 μm. In addition, the Cu_6Sn_5 in solder matrix just grew up under coupling stress without obvious migration and polarization effect. Therefore, the polarization effect could be reduced when the direction of electron flow and the direction of temperature gradient were opposite.

CONCLUSIONS

In this paper, the EM and TM behaviors of in line type of SAC0307 solder joints under thermoelectric coupling conditions were investigated and compared. The growth of IMC layer at the interfaces was mainly discussed at Sn-based solder joints with the *c*-axis nearly parallel to the current and thermal flow directions. Under the effect of EM, the evolution of interfacial IMC layers showed an obvious polarization effect in the solder joint. The thickness of the IMC layer at the anode increased 3.93 μm. Moreover, the Cu atoms tend to migrate from the hot side to the cold side. Thus, the thickness of the IMC layer at the cold side increased 1.72 μm. Under the thermoelectric coupling conditions, the migration direction of Cu atoms was influenced by the relative directions between EM and TM. When the EM and TM were in the same direction, namely + E_D and + T_D, the thickness of the IMC layer at the anode side (cold side) increased up to 7.67 μm, which indicated that the effect of thermal flow could assist to accumulate the IMC at the anode side, and accelerate the migration of Cu atoms. Under the condition of + E_D and − T_D, TM counteracted the effect of EM. The thickness of the IMC layer at the anode side just increased 0.2 μm. This research could help to further understand the reliability behaviors of SAC0307 solders under the service environment.

ACKNOWLEDGMENTS

The authors acknowledge the financial support of this study from the joint specialized research fund for the Beijing Natural Science Foundation (2162006 and 2170009), Beijing Young top notch talent support program (CIT&TCD201804007), and National Natural Science Foundation of China [Grant Numbers 51425101 and 51621003].

REFERENCES

1. T. Ohba, *ECS Trans.* 34, 1011 (2011).
2. R. Agarwal, W. Zhang, P. Limaye, R. Labie, B. Dimcic, A. Phommahaxay and P. Soussan, *2010 Proceedings 60th Electronic Components and Technology Conference (ECTC)*. June, vol. 858 (2010).
3. D.Q. Yu, J. Zhao, and L. Wang, *J. Alloy. Compd.* 376, 170 (2004).
4. H. Ye, C. Basaran, and D.C. Hopkins, *Appl. Phys. Lett.* 82, 1045–1047 (2003).
5. X. Gu, K.C. Yung, and Y.C. Chan, *J. Mater. Sci. Mater. Electron.* 21, 1090 (2010).
6. Y. Tian, J. Han, and F. Guo, *J. Mater. Sci.-Mater. Electron.* 28, 10785 (2017).
7. K.N. Tu, *J. Appl. Phys.* 94, 5451 (2003).
8. F.-Y. Ouyang, K.N. Tu, Y.-S. Lai, and A.M. Gusak, *J. Appl. Phys. Lett.* 89, 221906 (2006).
9. Y. Wang, J. Han, L.M. Ma, Y. Zuo, and F. Guo, *J. Electron. Mater.* 45, 6095 (2016).
10. G. Gurp, P. Waard, and F. Chatenier, *J. Appl. Phys.* 58, 728 (1985).
11. G. Gurp, P. Waard, and F. Chatenier, *J. Appl. Phys. Lett.* 45, 1054 (1984).
12. E. Stracke and C. Herzig, *Phys. Status Solidi (A)* 66, 189 (1981).
13. T.Y. Tan, *J. Appl. Phys. Lett.* 73, 2678 (1998).
14. P. Rimbey and R. Sorbello, *Phys. Rev. B Condens. Matter.* 38, 1095 (1988).
15. W.L. Schaich, *Phys. Rev. B.* 13, 3350 (1976).
16. A.M. Stoneham and C.P. Flynn, *J. Phys. F Metal Phys.* 3, 505 (1973).
17. R.A. Johns and D.A. Blackburn, *Thin Solid Films* 25, 291 (1975).
18. C.Q. Ru, *J. Mater. Sci.* 35, 5575 (2000).
19. W. Jones, *J. Phys. C Solid State Phys.* 14, 5505 (1981).
20. M.J. Gillan, *J. Phys. C Solid State Phys.* 17, L237 (1984).
21. M. Hamid and C. Basaran. *2008 33rd IEEE/CPMT IEMT*. (2008).
22. D. Feng, F. Wang, D. Li, B. Wu, and L. Liu, *Mater. Res. Express.* 6, 4 (2018).
23. F. Wang, H. Chen, D. Li, Z. Zhang, and X. Wang, *Electron. Mater. Lett.* 15, 1 (2018).
24. T. Tian, K.N. Tu, H.Y. Chen, H.Y. Hsiao, and C. Chen, *Annu. Rev. Mater. Res.* 40, 423 (2012).
25. A.T. Huang, K.N. Tu, and Y.-S. Lai, *J. Appl. Phys.* 100, 033512 (2006).
26. Y. Zuo, L.M. Ma, F. Guo, L. Qiao, Y.T. Shu, A. Lee, and K.N. Subramanian, *J. Electron. Mater.* 43, 4395 (2014).
27. Y. Tian, J. Han, L.M. Ma, and F. Guo, *Microelectron. Reliab.* 80, 7 (2018).
28. F. Guo, Q. Liu, L. Ma, and Y. Zuo, *J. Mater. Res.* 1, 1 (2016).
29. D. Yang, B.Y. Wu, Y.C. Chan, and K.N. Tu, *J. Appl. Phys.* 102, 043502 (2007).
30. C.M. Chen, L.T. Chen, and Y.S. Lin, *J. Electron. Mater.* 36, 168 (2007).
31. X. Gu, D. Yang, Y.C. Chan, and B.Y. Wu, *J. Mater. Res.* 23, 2591 (2011).
32. Z. Sun, L. Ma, Y. Wang, J. Han, Y. Zuo and F. Guo, *2017 18th International Conference on Electronic Packaging Technology (ICEPT)*. 750 (2017).
33. Y. Li, F.S. Wu, and Y.C. Chan, *J. Mater. Sci.-Mater. Electro.* 26, 8522 (2015).
34. H.-Y. Hsiao and C. Chen, *J Appl Phys Lett.* 90, 249902 (2007).